Processing and Application of Ceramics 15 [1] (2021) 69–78
https://doi.org/10.2298/PAC2101069D

Chelating agent and substrate effect on hydrothermal growth of Yb^{3+}/Er^{3+} doped $NaYF_4$ film

Suman Duhan[1], Kedar Sahoo[2], Md. Imteyaz Ahmad[3], Sudhir Kumar Singh[1], Manoj Kumar[2,*]

[1]*Department of Chemical Engineering, Thapar Institute of Engineering and Technology, Patiala, Punjab, India*
[2]*Department of Chemical Engineering and Technology, Indian Institute of Technology, Banaras Hindu University, Varanasi-221005, India*
[3]*Department of Ceramic Engineering, Indian Institute of Technology, Banaras Hindu University, Varanasi-221005, India*

Received 4 September 2020; Received in revised form 29 December 2020; Aaccepted 10 February 2021

Abstract

We report simultaneous crystal growth and deposition of upconverting Yb^{3+}/Er^{3+} doped $NaYF_4$ film (UCF) on conducting and non-conducting substrates by one-step hydrothermal method. The characteristics such as film topography, morphology, crystallographic phase and upconverting luminescence intensity were found to depend both on the chelating agent and nature of the substrate. The characteristics of the prepared films varied interestingly when either the chelating agent or the substrate was changed. The upconversion emission intensities were found to increase with decreasing film roughness. Further, current investigation demonstrated that the $NaYF_4$ films deposited using EDTA or DTPA chelating agents on ITO substrate and EGTA chelating agent on PG substrate were more uniform and resulted in greater upconverted emission intensities. We envision plausible use of current technology in the development of affordable optical platforms for several optoelectronic applications.

Keywords: *upconverting films, doped $NaYF_4$, hydrothermal synthesis, effect of substrate and chelating agent*

I. Introduction

Upconverting (UC) materials absorb multiple low-energy photons (wavelength in the order of 980 nm) to emit a high energy photon (400–700 nm). It finds extensive applications in the areas of photothermal and photodynamic therapy [1,2], nanothermometers [3], imaging labels [4], heavy metal detection [5] and multiplex biosensing [6]. Additionally, UC materials are being projected as a promising material for applications in the areas of multilayer optical storage disks [7], photoluminescent display screen [8], photovoltaic cells [9,10], diagnostics platform [11], improved cell culture analysis devices [12], optical security systems [13] and optical waveguides [14] requiring development of novel upconverting films (UCF) on the desired substrates.

Several processing methods for growing rare-earth doped upconverting platforms have been reported using thin-film deposition techniques, such as layer by layer deposition (LBL) [15], dip-coating [16], pulsed laser deposition (PLD) [17–19], spin coating [20], thermal evaporation [21] electron-beam vaporization [14], etc. However, these technologies start with an already synthesized upconverting base material, which are subsequently processed to make films. Further, LBL, PLD, electron-beam vaporization require high capital cost, sophisticated instrumentation and dedicated workforce. Additionally, rare-earth doped $NaYF_4$ upconverting films are difficult to synthesize by these conventional techniques due to the presence of fluorine and difficulty in formation of hexagonal phase at low temperature [22]. Applications requiring the development of affordable platforms can not utilize these cost-intensive techniques. In such cases, affordable synthetic methods such as hydrothermal processing would be a more viable choice for preparation of the phase pure upconvert-

*Corresponding author: tel: +918283839972,
e-mail: *manojk.che@iitbhu.ac.in*

ing platforms with high degree of crystallinity [23].

Hydrothermal method has been a popular [24–26] technique for thin-film deposition on various substrates, for example, deposition of Sb_2S_3 on indium tin oxide [27], high quality nanocrystalline CdZnS film on plain glass slide [28] and β-LaS_2 on stainless steel [29]. Also, the hydrothermal process is simple to use and enables the formation of highly crystalline films, with potential for large scale preparations, in a fewer number of steps as compared to other techniques [30–32]. As a result, material processing cost is significantly reduced. In the multitude of applications where UC materials can be employed as films such as energy harvesting or displays or diagnostic platforms, temperature and length of reaction time are known to alter film characteristics such as thickness, phase and crystallinity. Apart from other parameters, substrates and chelating agents have also been reported to have strong influence on the synthesized film characteristics such as film coverage, crystallinity, phase purity, film thickness and roughness [33–36]. Especially crystal growth and morphology of film can be controlled by varying surface charge of associated substrate [37]. Though a number of methods have been adopted for synthesis of upconverting films as discussed above, work related to deposition of UC materials over different substrates is very limited.

$NaYF_4$:Yb^{3+}/Er^{3+} system has become popular due to its ability to absorb two low energy photons in the NIR region, producing light emission in the visible region. $NaYF_4$ acts as an efficient host lattice and is known to be one of the most efficient upconverter due to low phonon-photon coupling [38]. Additionally, it stimulates the energy transfer process and controls the environment around dopant ions that influence the upconversion luminescence mechanism. Doping this host lattice with Yb^{3+} (sensitizer) improves the absorption in NIR region due to the large absorption cross-section (980 nm), and transfer of energy from the excitation source towards activator (Er^{3+}), ultimately generating light in the visible range. By Er^{3+} doping, emission ranging from green to red can be obtained since it has the characteristic emission bands centred at 540 and 650 nm [39]. Moreover, it is known that Yb^{3+}/Er^{3+} doped $NaYF_4$ exists in two polymorphs: α (cubic) and β (hexagonal) and among two, the hexagonal phase is known to have superior upconversion efficiency [38].

Current report, therefore, discusses the development of upconverting film (UCF) over the various substrates by hydrothermal method and correlates the change in emission intensity from $NaYF_4$:Yb^{3+}/Er^{3+} system with respect to the synthesis parameters and film characteristics such as chelating agent, substrate material, film microstructure and topography. Herein, we used three different chelating agents (ethylene diamine tetraacetic acid EDTA, ethylene glycol tetraacetic acid EGTA and diethylene triamine pentaacetic acid DTPA) and three different substrates (conducting indium tin oxide ITO and fluorinated tin oxide FTO and non-conducting plain glass PG). In the current study, both conducting and non-conducting transparent substrates were selected to cover applicability in a diverse range of applications: from imaging to photovoltaic.

II. Experimental

Yttrium chloride hexahydrate ($YCl_3 \cdot 6H_2O$), ytterbium chloride hexahydrate ($YbCl_3 \cdot 6H_2O$) and erbium chloride hexahydrate ($ErCl_3 \cdot 6H_2O$) were purchased from Sigma Aldrich, India. Sodium fluoride (NaF), ethylene glycol tetraacetic acid (EGTA), ethylene diamine tetraacetic acid (EDTA) and diethylene triamine pentaacetic acid (DTPA), all 99.99% pure, were procured from SRL Chemicals, India. All chemicals were of analytical grade and used without further purification. Conducting and non-conducting glass slides were purchased from Techinstro Pvt. Ltd., India.

All glass substrates (ITO, FTO and PG) were cut into 1.5 × 1.5 cm sizes and cleaned in warm (50 °C) concentrated nitric acid for ~15 min followed by washing 2–3 times in deionized water (DI = 18 MΩ/cm) and acetone. Subsequently, the substrates were dried at room temperature in a desiccator. Finally cleaned substrates were etched using dilute hydrofluoric acid (HF) solution for 5 s followed by deionized water washing and drying.

Upconverting films were obtained using a well-established hydrothermal protocol with some modifications [40]. Briefly, 0.2 M stock solutions of $YbCl_3$, YCl_3, $ErCl_3$ and chelating agents (i.e. EDTA, EGTA and DTPA), and 0.83 M solution of NaF were prepared. From the stock solutions, 0.17 mmol of $YbCl_3$, 0.80 mmol of YCl_3, 0.03 mmol of $ErCl_3$, and 1 mmol of the chelating agent (CA) were mixed for 30 min in a glass vial. After 30 min of mixing, 12.4 mmol of NaF was added to the solution and transferred to a Teflon lined stainless steel autoclave. The cleaned and etched substrate was fully submerged in the solution, closed inside the autoclave. The autoclave was sealed and placed in a preheated oven at 140 °C for 15 h. After completion of the reaction, the autoclave was cooled to the room temperature, and the substrate was washed with deionized water under sonication. The different UCFs were prepared using combination of various chelating agents (CA) and substrate (S) and have the following notation - UCF@S_CA (for example, notation for the UCF on ITO substrate prepared using EDTA is UCF@ITO_EDTA).

The crystallinity and crystallographic phases of the films were evaluated using X-ray diffraction (Rigaku Smart Lab diffractometer, Miniflex), using CuKα radiation source (λ = 1.54 Å), 2θ ranging from 10° to 80° at a scanning rate of 5 °/min and 0.02 °/min step size. Surface morphologies of the deposited films were analysed by scanning electron microscopy (SEM, FEI NOVA NANOSEM 450). The surface topography was studied using atomic force microscopy (AFM, Veeco, USA) in the tapping mode. For analysis, 10×10 μm area scans were obtained. The images were acquired by ras-

terizing 256 × 256 points. For the statistical analysis 20 points (10 horizontal and 10 vertical) were considered.

The luminescence spectra of the films were recorded in a spectrofluorometer (Horiba, Quanta master 400-PTI, Canada) using 980 nm continuous wave (CW) diode laser (PSU-III-LED, 500 mW) as an excitation source. The luminescence spectrum was acquired with an emission slit opening of 0.4 mm and an integration time of 0.1 s.

III. Results

X-ray diffraction patterns (Fig. 1) of the deposited films matched with standard hexagonal (JCPDS Card No. 98-007-6718) $NaYF_4$ phase. It can be observed that the majority of XRD peaks belong to hexagonal β-$NaYF_4$ phase. However, the presence of NaF (JCPDF Card No. 98-004-8929) and the traces of cubic $NaYF_4$ (JCPDS Card No. 98-001-9092) are also confirmed. Formation of hexagonal β-$NaYF_4$ phase is in line with the proposed hypothesis of phase pure upconverting system prepared by hydrothermal reaction. Moreover, long reaction time and high-pressure condition inside the autoclave probably also favour the formation of hexagonal phase at a low temperature (140 °C). It has been reported earlier that thermal decomposition reaction at lower temperature produced cubic $NaYF_4$ phase which underwent transition through mixed phase (cubic and hexagonal) and ultimately converted to hexagonal phase at temperature above 300 °C [41,42]. Domination of hexagonal $NaYF_4$ phase in the UCFs prepared by the combination of various substrates and chelating ligands is possibly due to the absence of stabilization of small-sized α-$NaYF_4$ nuclei formed during dissolution recrystallization process, forming hexagonal phase, assisted by surface-attached ligand [43]. Since Yb^{3+}/Er^{3+} doped $NaYF_4$ in the hexagonal phase is known to have better upconversion efficiency, the hydrothermal process of film deposition was found to be more economical and less labour intensive.

In addition to the peaks corresponding to β-$NaYF_4$, three more peaks at $2\theta \sim 38.88°$, 56.14° and 70.39° belonging to NaF appeared for all UCFs. It is noted that no peak corresponding to the YF_3 is observed in any of UCFs, which indicates that the NaF is not a decomposition product. It is important to note that NaF is major constituent of $NaYF_4$ host lattice and responsible for the photon-phonon interaction. Hence NaF added quantity was ~4 times in excess to YCl_3 to compensate for losses incurred during longer period of solution processing. Further, addition of excess NaF in the solution is known to play important role in controlling phase and morphology of resulting upconverting particles through accelerated crystallization process [44–46]. Since NaF was taken in high amount during synthesis, due to the reaction in longer period, it precipitated and was detected from X-ray diffraction peaks.

The peaks corresponding to NaF varied in intensity with substrate and chelating agent variation depending upon coordinating capability of ligand for rare earth ions and subsequent precipitation of extra NaF dissolved in solution. Octadentate DTPA ligand having high formation constant as compared to EDTA and EGTA, chelates better with Re^{3+} ions. During synthesis improved chelation of Re^{3+} ions and subsequent bond weakening, results in primary nucleation followed by crystal growth and stabilization. Additionally, the bulky DTPA facilitates faster aggregation of unstable smaller nuclei during crystal growth process. Thus, rapid nucleation and subsequent stabilization of the formed crystals during UCF synthesis result in more unconsumed NaF precursor (Fig. 1c). Besides sparingly soluble DTPA as compared to EDTA and EGTA makes the former ligand as limiting reactant, thus amount of NaF used during synthesis is not utilized completely for crystal formation (confirmed by XRD results).

SEM micrographs of the UCFs on three types of substrates (PG, ITO and FTO) employing three different chelating agents (DTPA, EDTA and EGTA) are depicted in Fig. 2. In general, Yb^{3+}/Er^{3+} doped $NaYF_4$ films on various substrates seem to consist of two parts: a compact thin layer in contact with the substrate and the second layer of isolated well faceted hexagonal or equiaxed particles (sizes ~1 μm in the lateral direction). SEM im-

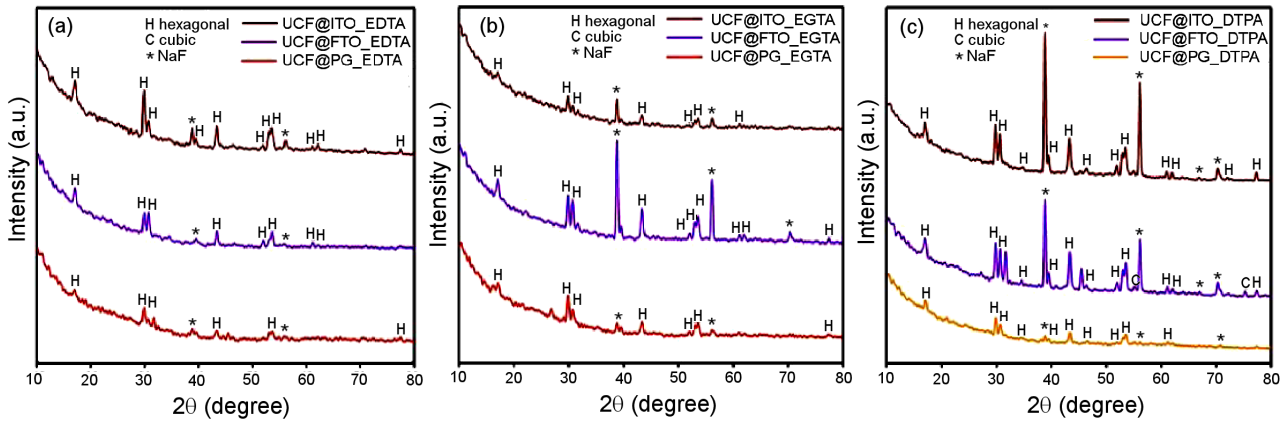

Figure 1. X-ray diffraction patterns of UCF over various substrates, prepared using: a) EDTA, b) EGTA and c) DTPA as chelating agent

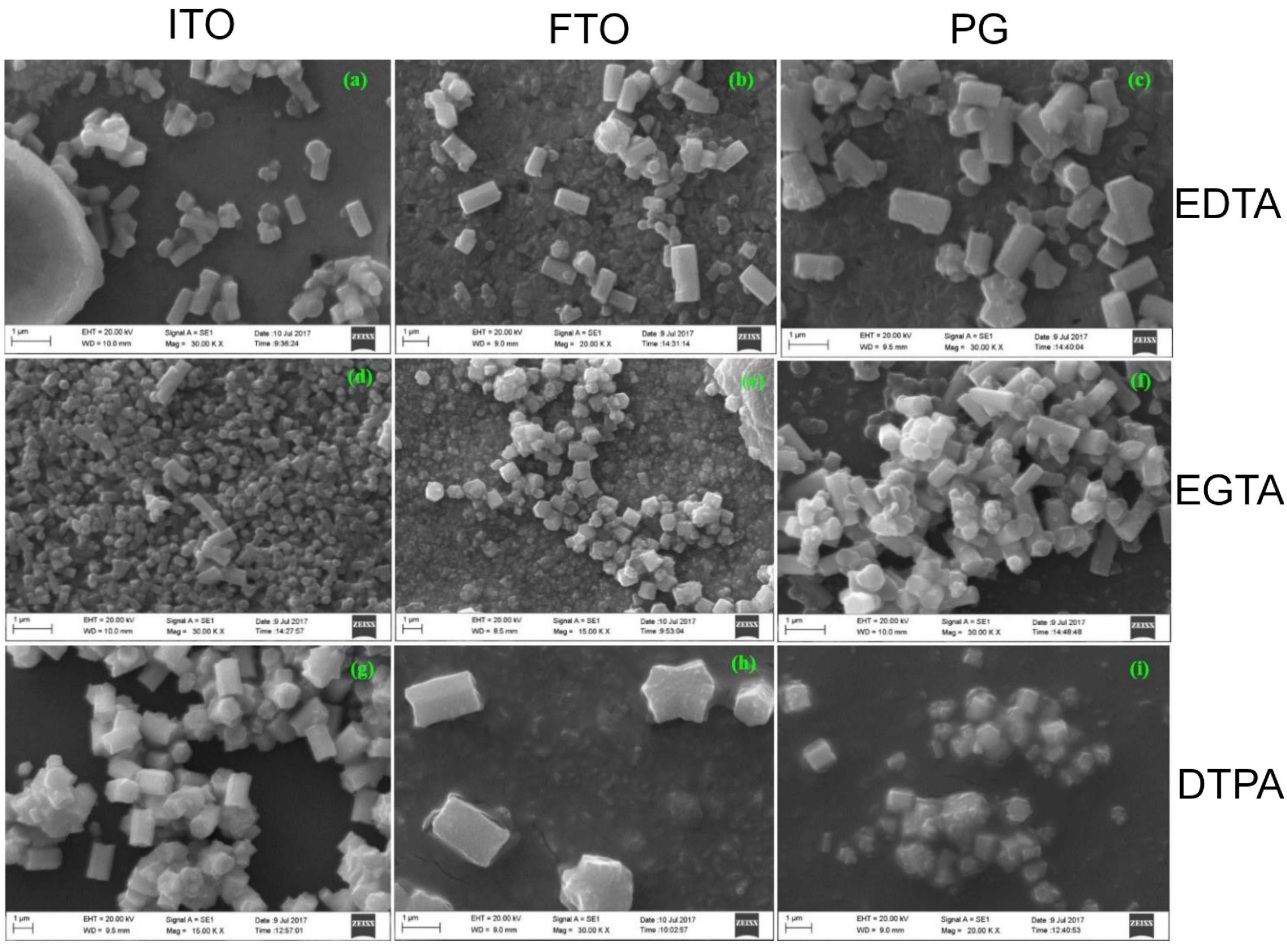

Figure 2. SEM images of isolated upconverting particles over the UCF: a) UCF@ITO_EDTA, b) UCF@FTO_EDTA, c) UCF@PG_EDTA, d) UCF@ITO_EGTA, e) UCF@FTO_EGTA, f) UCF@PG_EGTA, g) UCF@ITO_DTPA, h) UCF@FTO_DTPA and i) UCF@PG_DTPA

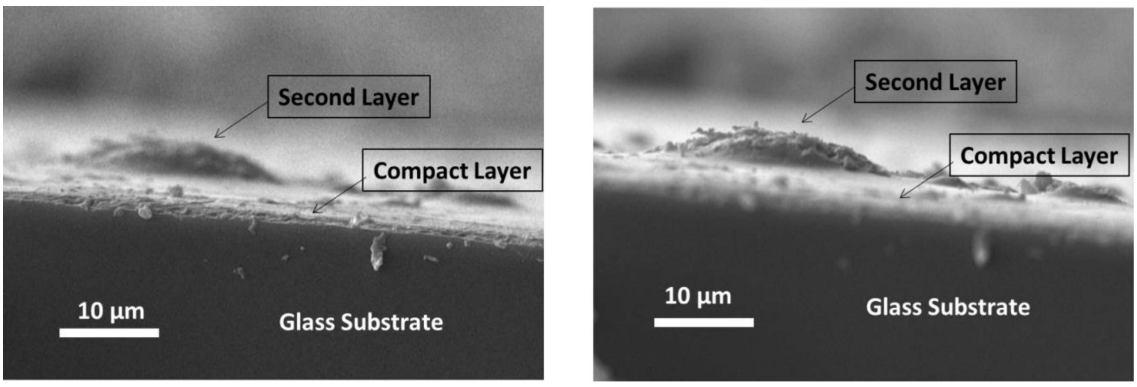

Figure 3. Cross sectional SEM images of the fractured surface of the prepared UCF

ages of the cross-section of the UCFs (Fig. 3) may indicate formation of compact layer of nanostructure attached to the substrate followed by growth of larger upconverting particles upon it. This could be an indication of the probable growth mechanism of the films where the islands of upconverting particles clusters may have formed initially merging to give a dense uniform film or vice-versa during continuous growth process (Fig. 3). It is important to note that since there was no unusual phases, and crystallinity was observed in the case of the prepared UCFs, it is expected that no compositional difference exists between two layers.

In the case of EDTA as a chelating agent, the films deposited on FTO and PG substrates appeared similar, with uniform background coverage layer and identical hexagonal faceted grains (Figs. 2b and 2c), while the coverage of the films was not good when deposited on ITO substrate and isolated chunks were observed (Fig. 2a). The films deposited on all the substrates, using EGTA as a cheating agent, exhibited good surface

coverage with varying morphology. The grains were equiaxed for the films deposited on FTO substrate (Fig. 2e) while on the other hand, ITO and PG substrates displayed elongated hexagonal morphology (Figs. 2d and 2f), with much finer crystals in the case of ITO when compared to PG substrates. A glassy matrix around the particles could be observed in the case of films deposited on all substrates using DTPA as a chelating agent, while the films deposited using EDTA and EGTA chelating agents were much cleaner and well defined.

Generally, improved chelation capability of the ligand towards specific ion in precursor solution increases the energy barrier needed for nucleation. Thus, those ligands having strong chelation capacity require higher temperatures for crystallization [47]. The films processed with DTPA, being a stronger chelating agent, have a distinct glass-like underlying layer (Figs. 2h and 2i), which was not observed in the case of other two chelating agents (Figs. 2a-f). On the other hand, irrespective of the chelating agent, when the film was deposited on ITO substrate, crystals were well faceted and discontinuous while the film coverage was poor (Figs. 2a, 2d and 2g). This indicated the possible role of surface charge in controlling crystal growth and morphology [37].

It is noteworthy that the upconverting particles grown over different substrates are micro-rod/ cylindrical, disc, flower-like shape by use of various chelating ligands. However, the upconverting particles formed by EDTA ligands are cylindrical or micro-rod shaped. This can be correlated with the small molecular weight as well simple structure of the ligand as compared to EGTA and DTPA. Generally, ligand dynamics over the crystal surface has a strong tendency of controlling growth of Yb^{3+}/Er^{3+} doped $NaYF_4$ over substrate attached by coordination effect [48]. DTPA ligand is an expanded version of EDTA, based on diethylene triamine backbone with five carboxymethyl groups. Similarly, EGTA is an aminopolycarboxylic acid of EDTA, but has an elongated structure due to additional R–O–R linkage. These make EGTA and DTPA more complex and heavier moieties as compared to EDTA. Generally, smaller ligand has a greater tendency of leaving the crystal surface rapidly during hydrothermal synthesis, facilitating directional growth aligned along a certain crystallographic axis. This is clearly visible in the case of the upconverting particles synthesized by EDTA over various substrates depicting nearly micro-rod/cylindrical morphology. Initially, there is a formation of flowerlike aggregation due to faster leaving of the adsorbed ligand

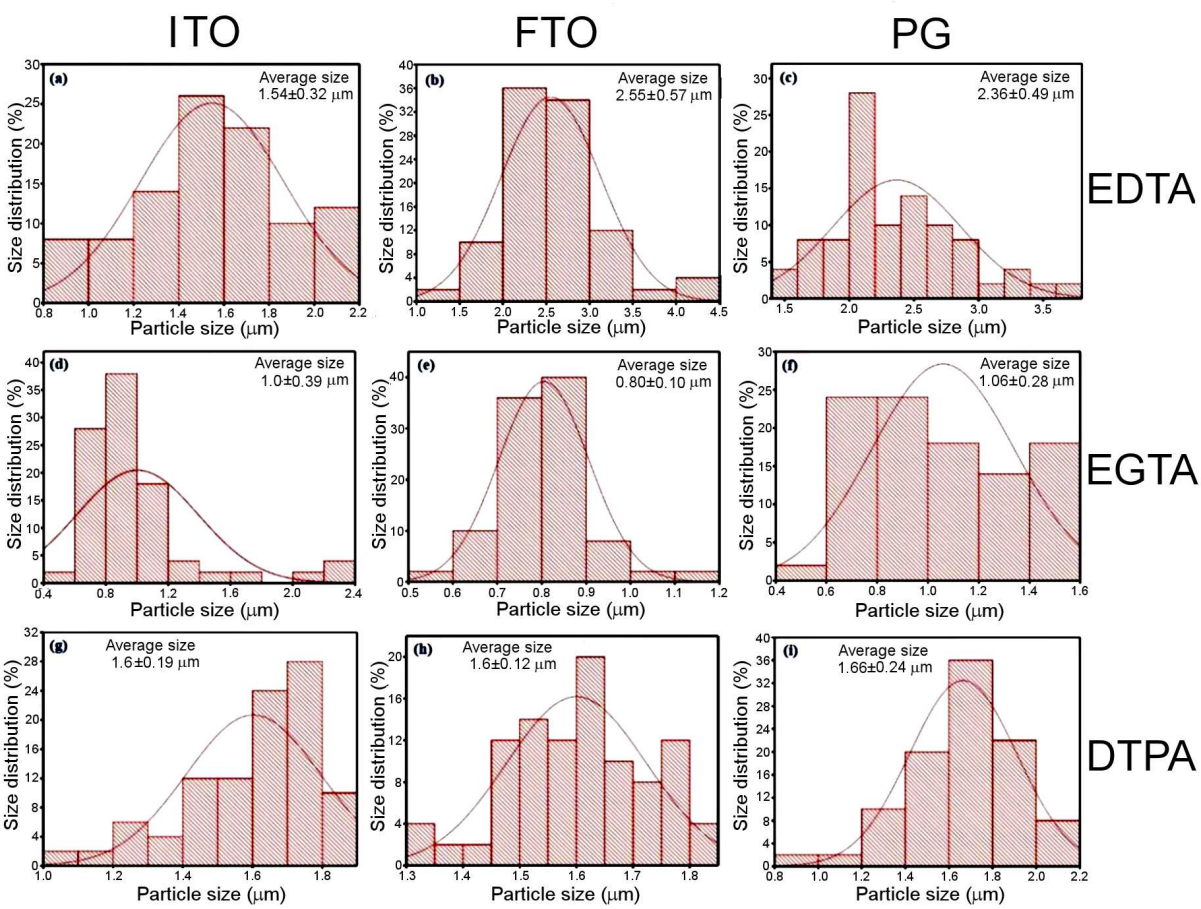

Figure 4. Size distribution analysis of upconverting particles synthesized over various substrates in combination with different chelating agents: a) UCF@ITO_EDTA, b) UCF@FTO_EDTA, c) UCF@PG_EDTA, d) UCF@ITO_EGTA, e) UCF@FTO_EGTA, f) UCF@PG_EGTA, g) UCF@ITO_DTPA, h) UCF@FTO_DTPA and i) UCF@PG_DTPA

from a crystal surface, thus making its surface unstable. Subsequently aggregated nuclei in combination with reactant media resulted in full-grown crystal which subsequently formed flower-like structure as observed on the plain glass substrate. After a certain growth, extrusion leads to rod like morphology. Whereas, in the case of DTPA and EGTA, due to large molecular structure, the tendency of leaving crystal surface during reaction stage is lower. Therefore, crystals grown along lateral direction forming disc or plate-like hexagonal structure have small aspect ratio. However, due to nearly comparable molecular backbone, there is no distinct morphological difference between the films synthesized using EDTA, DTPA and EGTA. Additionally, the unstable surface dynamics of crystals during their dissolution in the reaction media results in the formation of irregular morphologies. Furthermore, the size distribution analysis (Fig. 4) provided insight into the various factors controlling the upconverting particles growth on different substrates.

SEM results revealed micron-sized particles with varying morphology, grown over conducting/non-conducting substrates, depending upon chelating ligand used. EDTA and DTPA ligands produced large-sized particles as compared to EGTA-assisted synthesis. The small-sized upconverting particles resulted from EGTA-assisted synthesis may be correlated with the long chain length of EGTA molecule which have a tendency of stabilizing small-sized nuclei formed during the initial phase of synthesis. These surface stabilized nuclei have a weaker tendency of dissolution in hydrothermal reaction mixture thus inhibit the growth of large-sized nuclei during subsequent crystallization. Notice that EDTA is relatively simple in structure and hence has a greater tendency of leaving crystal surface, with high surface dynamics. Similarly, bulkier DTPA facilitates aggregation of nuclei during the crystal growth process as small nuclei are not stable. Hence improved surface dynamics as well as large-sized nuclei helped in the formation of bigger sized upconverting particles.

The topography of the films was investigated using atomic force microscopy (AFM) in tapping mode. The maximum roughness of the film surface was found to be within 60 nm. The average roughness (R_a) and interface width or root means square roughness (RMS), were statistically analysed. Here, R_a indicates the absolute average distance of the surface point with respect to the mean plane. RMS value indicates the standard deviation of the surface with reference to mean plane [48]. The images in Fig. 5 show nine different UCFs with sample heights (from the mean plane) ranging from 30 to 300 nm. Each figure panel was divided into central quadrant showing 3D profile, top left quadrant indicating surface topography and the top right quadrant displaying grain size. The analysed R_a and RMS values are summarized in Table 1.

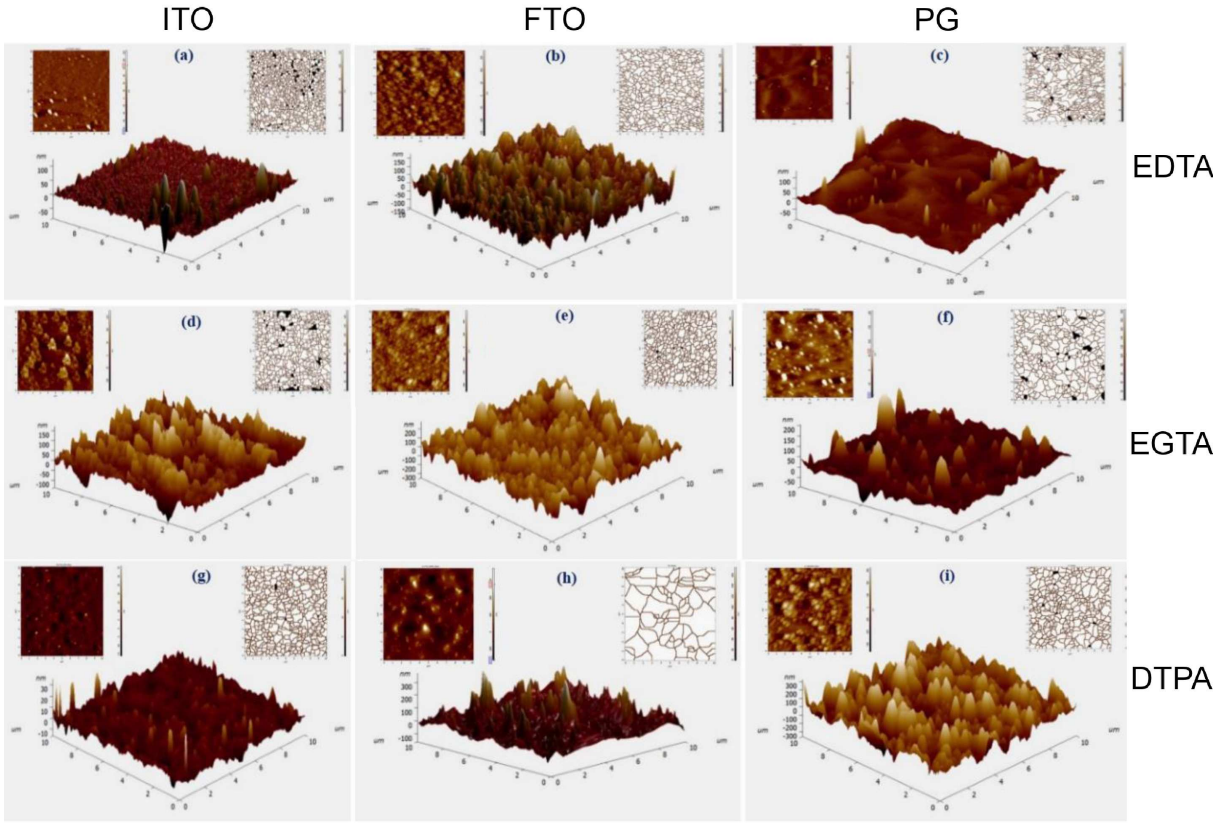

Figure 5. AFM images of UCF along with surface topography: a) UCF@ITO_EDTA, b) UCF@FTO_EDTA, c) UCF@PG_EDTA, d) UCF@ITO_EGTA, e) UCF@FTO_EGTA, f) UCF@PG_EGTA, g) UCF@ITO_DTPA, h) UCF@FTO_DTPA and i) UCF@PG_DTPA

Table 1. The statistical parameters (average roughness R_a and root means square roughness *RMS*) related to thin-film calculated based on AFM images

Chelating Agent	Substrate	*RMS* [nm]	R_a [nm]
EDTA	ITO	5.83	4.34
	FTO	34.41	27.83
	PG	9.91	7.46
EGTA	ITO	34.88	27.46
	FTO	57.32	44.18
	PG	17.65	12.88
DTPA	ITO	3.05	2.39
	FTO	47.3	38.65
	PG	58.54	46.01

It is observed that *RMS* and R_a values of the films prepared by any chelating agent depend on the used substrate. It is evident that while using EDTA and DTPA as chelating agents, minimum film roughness (*RMS* and R_a) was observed from the UCF deposited on ITO substrate. At the same time, when EGTA was used as a chelating agent, films deposited on PG substrate had minimum roughness. UCF obtained with EDTA over FTO (Fig. 5b) displayed relatively broad surface roughness profile when compared to that of those grown on ITO (Fig. 5a) and PG (Fig. 5c) substrates. Additionally, EGTA-assisted UCF displayed sharper surface roughness profiles as observed in the case of PG substrate (Fig. 5f). Further, it can be seen that the films grown on FTO (Fig. 5h) and PG (Fig. 5i) using DTPA as a chelating agent exhibited relatively broad peaks with substrate surface irregularities, but film deposited on ITO (Fig. 5g) displayed sharp peaks. All DTPA-assisted UCFs resulted in greater root-mean-square roughness values. Further, statistical data suggest relatively weak substrate effects on the morphology when compared with the effect of the chelating agents, as mentioned earlier. However, to study the effect of original substrate roughness, AFM analysis of etched plain glass slide was acquired. Root mean square (*RMS*) and average (R_a) roughness of the etched glass substrate ($10 \times 10\,\mu m$) was found to be ~75 and ~51 nm, respectively. *RMS* and R_a of different UCFs deposited over plain glass substrate have lower values (Table 1), indicating the formation of good upconverting layer on the used substrates.

The thin films deposited over conducting and non-conducting substrates were investigated for the photoluminescence upon excitation by 980 nm radiation using inexpensive continuous-wave diode laser. This results in five upconverted luminescence bands at wavelengths 390, 410, 525, 540 and 650 nm (Fig. 6), which were attributed to $^4G_{11/2} \rightarrow {}^4I_{15/2}$, $^2H_{9/2} \rightarrow {}^4I_{15/2}$, $^2H_{11/2} \rightarrow {}^4I_{15/2}$, $^4S_{3/2} \rightarrow {}^4I_{15/2}$ and $^4F_{9/2} \rightarrow {}^4I_{15/2}$ transition states, respectively [27]. It is important to mention that Yb^{3+} being sensitizer absorbs the NIR radiation and transfers to closely lying proximal Er^{3+} ions present in the $NaYF_4$ lattice, resulting in characteristic upconversion emission (Fig. 6). This characteristic upconverted emission is a strong indication of the efficient incorporation of Yb^{3+} and Er^{3+} in $NaYF_4$ structure and successful formation of upconverting films.

The qualitative comparison of characteristic luminescence intensity of $NaYF_4$:Yb^{3+}/Er^{3+} films on different substrates for the same chelating agent is given in Table 2. It is interesting to note that the highest luminescence intensity was observed in the case of the films deposited on ITO substrates when DTPA and EDTA were used as chelating agents. On the other hand, when EGTA chelating agent was employed, the film deposited on PG substrate showed the highest luminescence intensity. The effect of chelating agent on different substrates is summarized in Table 3. EGTA chelating agent re-

Table 2. Effect of the chelating agent on characteristic luminescence intensity deposited on different substrates

Chelating agent	Luminescence intensity (decreasing order)
EDTA	ITO>PG>FTO
EGTA	PG>FTO>ITO
DTPA	ITO>FTO>PG

Table 3. Effect of substrate on the characteristic luminescence intensity from UCFs with different chelating agents

Substrate	Luminescence intensity (decreasing order)
ITO	DTPA>EDTA>EGTA
FTO	EGTA>DTPA>EDTA
PG	EGTA>EDTA>DTPA

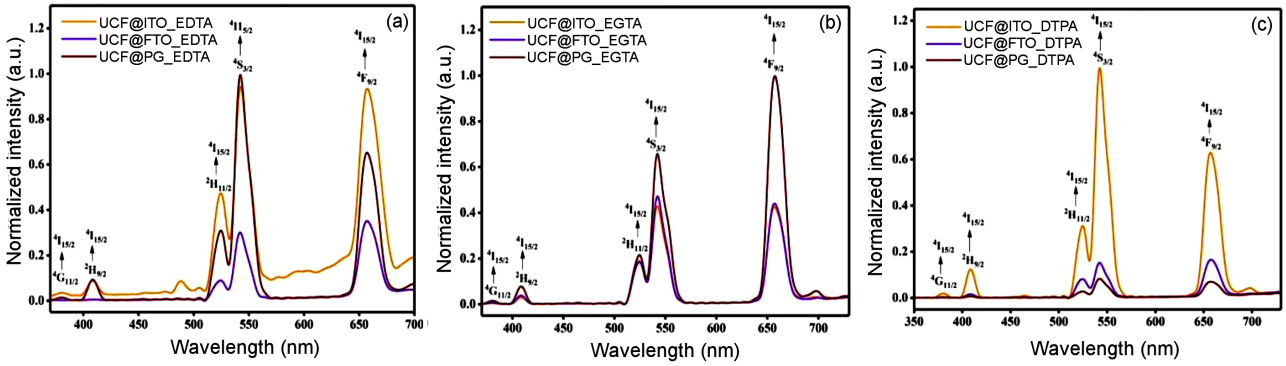

Figure 6. Luminescence spectra of UCF prepared using: a) EDTA, b) EGTA and c) DTPA as chelating agents

sulted in the highest luminescence intensity for the films deposited on FTO and PG substrates, while the lowest luminescence intensity was observed for the films deposited on ITO substrate. The results from Tables 2 and 3 clearly demonstrate that both chelating agent and substrate have a pronounced effect on the upconverting emission characteristic of the films.

It is also concluded that the roughness of the deposited films has a direct correlation with luminescence behaviour. This is because of the fact that the film roughness can result in diffused scattering, reducing effective luminescence cross-section, thereby, suppressed luminescence intensity was observed. Smoother films resulted in higher luminescence intensities, while the luminescence intensity decreased with increasing roughness. For instance, in the case of the films prepared using DTPA, very smooth film having *RMS* value of around 3 nm was obtained when deposited on ITO. On the other hand, using same chelating agent films deposited on FTO and PG were much rougher having *RMS* roughness value around 47 and 57 nm, respectively. Accordingly, the luminescence intensity (Fig. 6c) obtained from the UCF deposited on ITO was very high when compared to that obtained from the UCFs deposited on FTO or PG substrate. Similarly, in the case of UCF prepared by EDTA and EGTA as chelating agents on ITO and PG substrates, the samples have the lowest *RMS* roughness values, which resulted in highest luminescence intensity. The above study showed that film roughness depends both on the nature of chelating agent and substrate used. Best luminescence intensity was observed from the films deposited on ITO substrate and DTPA as the chelating ligand.

As per early reports by Giedraityte *et al.* [49] the upconversion intensity is independent of film thickness. Thus, the film thickness may not have significant role in tuning upconversion emission intensity in the current study. It is observed that film thickness of the UCFs varied slightly with change in nature of chelating agent and is about 3 μm, as shown in Fig. 7.

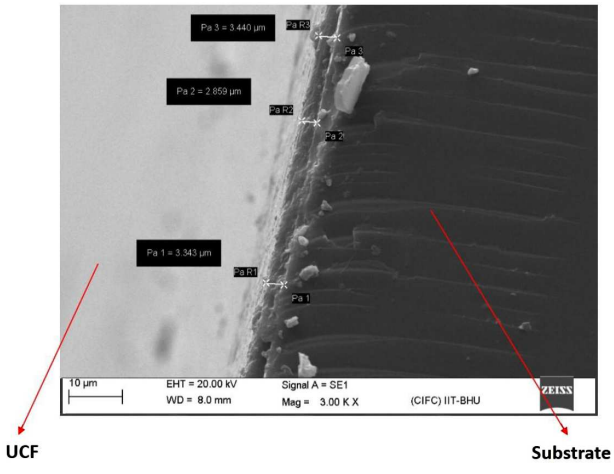

Figure 7. SEM image of the cross section of prepared UCF showing formation of micron sized film over substrate

IV. Conclusions

In conclusion, $NaYF_4$:Yb^{3+}/Er^{3+} upconverting films (UCFs) were deposited by low temperature, facile, one-step hydrothermal process. The film characteristics changed interestingly when either substrate or the chelating agent was changed, showing that both substrate and chelating agent affected the film characteristics such as phase formation, roughness and luminescence intensity. The best emission intensities on the non-conducting substrate were achieved by using EGTA as a chelating agent. Further, in the case of conducting substrates, combination of EGTA ligand with FTO substrate and DTPA ligand with ITO substrate produced upconverting films with improved luminescence intensities.

Acknowledgements: We thank Department of Science and Technology, New Delhi, (Nano Mission: SR/NM/NS-1320/14-15) and Center of Energy Resource Development, IIT (BHU) Varanasi for funding this work. We also sincerely thank Central Instrumentation facility (CIF) IIT (BHU) for characterizing our samples.

References

1. P. Zhang, W. Steelant, M. Kumar, M. Scholfield, "Versatile photosensitizers for photodynamic therapy at infrared excitation", *J. Am. Chem. Soc.*, **129** [15] (2007) 4526–4527.
2. X. Zhu, W. Feng, J. Chang, Y.W. Tan, J. Li, M. Chen, Y. Sun, F. Li, "Temperature-feedback upconversion nanocomposite for accurate photothermal therapy at facile temperature", *Nature Commun.*, **7** (2016) 10437.
3. F. Vetrone, R. Naccache, A. Zamarrón, A. Juarranz de la Fuente, F. Sanz-Rodríguez, L. Martinez Maestro, E. Martín Rodriguez, D. Jaque, J. García Solé, J.A. Capobianco, "Temperature sensing using fluorescent nanothermometers", *ACS Nano*, **4** [6] (2010) 3254–3258.
4. F. Wang, D. Banerjee, Y. Liu, X. Chen, X. Liu, "Upconversion nanoparticles in biological labeling, imaging, and therapy", *Analyst.*, **135** [8] (2010) 1839–1854.
5. M. Kumar, P. Zhang, "Highly sensitive and selective label-free optical detection of mercuric ions using photon upconverting nanoparticles", *Biosens. Bioelectron.*, **25** [11] (2010) 2431–2435.
6. S. Wu, N. Duan, Z. Shi, C. Fang, Z. Wang, "Simultaneous aptasensor for multiplex pathogenic bacteria detection based on multicolor upconversion nanoparticles labels", *Anal. Chem.*, **86** [6] (2014) 3100–3107.
7. H.P. Ho, W.W. Wong, S.Y. Wu, K.C. Lo, Y. Chan, W.W. Lam, E.E. Pun, "Multilayer optical storage disc based on the frequency up-conversion effect from rare earth ions", *Jpn. J. Appl. Phys.*, **41** [6A] (2002) L641–L643.
8. Q.H. Wang, M. Bass, "Photo-luminescent screens for optically written displays based on upconversion of near infrared light", *Electron. Lett.*, **40** [16] (2004) 987–988.
9. A. Shalav, B. Richards, T. Trupke, K. Krämer, H.U. Güdel, "Application of $NaYF_4$:Er^{3+} up-converting phosphors for enhanced near-infrared silicon solar cell response", *Appl. Phys. Lett.*, **86** [1] (2005) 013505.
10. B. Richard, A. Shalav, "The role of polymers in the luminescence conversion of sunlight for enhanced solar cell

performance", *Synthetic Metal.*, **154** [1-3] (2005) 61–64.
11. S.Y. Lee, M. Lin, A. Lee, Y.I. Park, "Lanthanide-doped nanoparticles for diagnostic sensing", *Nanomaterials*, **7** [12] (2017) 411.
12. S. Yang, W.H. Tse, J. Zhang, "Deposition of antibody modified upconversion nanoparticles on glass by a laser-assisted method to improve the performance of cell culture", *Nanoscale Res. Lett.*, **14** [1] (2019) 101.
13. W.J. Kim, M. Nyk, P.N. Prasad, "Color-coded multilayer photopatterned microstructures using lanthanide (III) ion co-doped $NaYF_4$ nanoparticles with upconversion luminescence for possible applications in security", *Nanotechnol.*, **20** [18] (2009) 185301.
14. J.M. Chwalek, G.R. Paz-Pujalt, "Upconverting Tm^{3+} doped Ba-Y-Yb-F thin film waveguides for visible and ultraviolet light sources", *Appl. Phys. Lett.*, **66** [4] (1995) 410–412.
15. Y. Bao, Q.A.N. Luu, C. Lin, J.M. Schloss, P.S. May, C. Jiang, "Layer-by-layer assembly of freestanding thin films with homogeneously distributed upconversion nanocrystals", *J. Mater. Chem.*, **20** [38] (2010) 8356–8361.
16. W. Huang, C. Lu, C. Jiang, W. Wang, J. Song, Y. Ni, Z. Xu, "Controlled synthesis of $NaYF_4$ nanoparticles and upconversion properties of $NaYF_4$:Yb, Er (Tm)/FC transparent nanocomposite thin films", *J. Colloid Interface Sci.*, **376** [1] (2012) 34–39.
17. C. Wang, X. Cheng, "Synthesis of a $NaYF_4$:Yb, Er upconversion film on a silicon substrate and its tribological behavior", *RSC Adv.*, **5** [115] (2015) 94980–94985.
18. G. Qin, W. Qin, C. Wu, S. Huang, J. Zhang, S. Lu, D. Zhao, H. Liu, "Enhancement of ultraviolet upconversion in Yb^{3+} and Tm^{3+} codoped amorphous fluoride film prepared by pulsed laser deposition", *J. Appl. Phys.*, **93** [7] (2003) 4328–4330.
19. G. Qin, W. Qin, S. Huang, C. Wu, D. Zhao, B. Chen, S. Lu, E. Shulin, "Infrared-to-violet upconversion from Yb^{3+} and Er^{3+} codoped amorphous fluoride film prepared by pulsed laser deposition", *J. Appl. Phys.*, **92** [11] (2002) 6936–6938.
20. C. Lin, M.T. Berry, R. Anderson, S. Smith, P.S. May, "Highly luminescent NIR-to-visible upconversion thin films and monoliths requiring no high-temperature treatment", *Chem. Mater.*, **21** [14] (2009) 3406–3413.
21. Z. Jia, K. Zheng, D. Zhang, D. Zhao, W. Qin, "Upconversion emission from Yb^{3+} and Tm^{3+} codoped $NaYF_4$ thin film prepared by thermal evaporation", *J. Nanosci. Nanotech.*, **11** [11] (2011) 9690–9692.
22. H. Jia, Y. Zhou, X. Li, Y. Li, W. Zhang, H. Fu, J. Zhao, L. Pan, X. Liu, J. Qiu, "Synthesis and phase transformation of $NaGdF_4$:Yb-Er thin films using electro-deposition method at moderate temperatures", *Cryst. Eng. Commun.*, **20** [43] (2018) 6919–6924.
23. Y. Zhang, L. Zhang, R. Deng, J. Tian, Y. Zong, D. Jin, X. Liu, "Multicolor barcoding in a single upconversion crystal", *J. Am. Chem. Soc.*, **136** [13] (2014) 4893–4896.
24. T. Dongale, S. Shinde, R. Kamat, K. Rajpure, "Nanostructured TiO_2 thin film memristor using hydrothermal process", *J. Alloys Compd.*, **593** (2014) 267–270.
25. T. Morita, Y. Wagatsuma, Y. Cho, H. Morioka, H. Funakubo, N. Setter, "Ferroelectric properties of an epitaxial lead zirconate titanate thin film deposited by a hydrothermal method below the Curie temperature", *Appl. Phys. Lett.*, **84** [25] (2004) 5094–5096.
26. K. Shimomura, T. Tsurumi, Y. Ohba, M. Daimon, "Preparation of lead zirconate titanate thin film by hydrothermal method", *Jpn. J. Appl. Phys.*, **30** [9S] (1991) 2174–2177.
27. W. Zhang, M. Tan, P. Zhang, L. Zhang, W. Dong, Q. Wang, J. Ma, E. Dong, S. Xu, G. Wang, "One pot synthesis of Sb_2S_3 nanocrystalline films through a PVP-assisted hydrothermal process", *Appl. Surf. Sci.*, **455** (2018) 1063–1069.
28. J. Mathew, E. Anila, "Hydrothermal assisted chemical bath deposition of (Cd:Zn)S thin film with high photosensitivity and low dark current", *Solar Energ.*, **172** (2018) 165–170.
29. T.T. Ghogare, R.B. Pujari, A.C. Lokhande, C.D. Lokhande, "Hydrothermal synthesis of nanostructured β-LaS_2 thin films", *Appl. Phys. A*, **124** [3] (2018) 248.
30. J. Chen, K. Huang, S. Liu, "Hydrothermal preparation of octadecahedron Fe_3O_4 thin film for use in an electrochemical supercapacitor", *Electrochim. Acta*, **55** [1] (2009) 1–5.
31. J.H. Kim, E.M. Kim, D. Andeen, D. Thomson, S.P. DenBaars, F.F. Lange, "Growth of heteroepitaxial ZnO thin films on GaN-buffered Al_2O_3 (0001) substrates by low-temperature hydrothermal synthesis at 90 °C", *Adv. Function. Mater.*, **17** [3] (2007) 463–471.
32. Y. Ohba, M. Miyauchi, E. Sakai, M. Daimon, "Hydrothermal syntheses of lead zirconate titanate thin films fabricated by a continuous-supply autoclave", *Jpn. J. Appl. Phys.*, **34** [part 1] (1995) 5216–5219.
33. S. Baruah, J. Dutta, "Hydrothermal growth of ZnO nanostructures", *Sci. Technol. Advance. Mater.*, **10** [1] (2009) 013001.
34. S. Baruah, C. Thanachayanont, J. Dutta, "Growth of ZnO nanowires on nonwoven polyethylene fibers", *Sci. Technol. Adv. Mater.*, **9** [2] (2008) 025009.
35. S.K. Das, S.N. Sahoo, S. Sarangi, P. Sahoo, "Substrate effect of hydrothermally grown ZnO nanorods and its luminescence properties", *J. Experiment. Nanosci.*, **8** [3] (2013) 382–388.
36. Z.N. Urgessa, O.S. Oluwafemi, J.R. Botha, "Hydrothermal synthesis of ZnO thin films and its electrical characterization", *Mater. Lett.*, **79** (2012) 266–269.
37. A.K. Dubey, H. Yamada, K.I. Kakimoto, "Surface charge induced enhanced crystallization on the piezoelectric sodium potassium niobate substrate", *J. Cryst. Growth*, **382** (2013) 7–14.
38. J. Suyver, A. Aebischer, D. Biner, P. Gerner, J. Grimm, S. Heer, K. Krämer, C. Reinhard, H.U. Güdel, "Novel materials doped with trivalent lanthanides and transition metal ions showing near-infrared to visible photon upconversion", *Optic. Mater.*, **27** [6] (2005) 1111–1130.
39. C. Chen, C. Li, Z. Shi, "Current advances in lanthanide-doped upconversion nanostructures for detection and bioapplication", *Advance. Sci.*, **3** [10] (2016) 1600029.
40. M. Kumar, Y. Guo, P. Zhang, "Highly sensitive and selective oligonucleotide sensor for sickle cell disease gene using photon upconverting nanoparticles", *Biosens. Bioelectron.*, **24** [5] (2009) 1522–1526.
41. G. Yi, H. Lu, S. Zhao, Y. Ge, W. Yang, D. Chen, L.H. Guo, "Synthesis, characterization, and biological application of size-controlled nanocrystalline $NaYF_4$:Yb, Er infrared-to-visible up-conversion phosphors", *Nano Lett.*, **4** [11] (2004) 2191–2196.
42. J.H. Zeng, J. Su, Z.H. Li, R.X. Yan, Y.D. Li, "Synthesis and upconversion luminescence of hexagonal-phase

$NaYF_4$:Yb, Er^{3+} phosphors of controlled size and morphology", *Adv. Mater.*, **17** [17] (2005) 2119–2123.
43. S. Wu, Y. Liu, J. Chang, S. Zhang, "Ligand dynamic effect on phase and morphology control of hexagonal $NaYF_4$", *Cryst. Eng. Commun.*, **16** [21] (2014) 4472–4477.
44. C. Liu, H. Wang, X. Li, D. Chen, "Monodisperse, size-tunable and highly efficient β-$NaYF_4$:Yb,Er(Tm) upconversion luminescent nanospheres: controllable synthesis and their surface modifications", *J. Mater. Chem.*, **19** [21] (2009) 3546–3553.
45. M. Ding, C. Lu, L. Cao, Y. Ni, Z. Xu, "Controllable synthesis, formation mechanism and upconversion luminescence of β-$NaYF_4$:Yb^{3+}/Er^{3+} microcrystals by hydrothermal process", *Cryst. Eng. Commun.*, **15** [41] (2013) 8366–8373.
46. S. Liu, G. De, Y. Xu, X. Wang, Y. Liu, C. Cheng, J. Wang, "Size, phase-controlled synthesis, the nucleation and growth mechanisms of $NaYF_4$:Yb/Er nanocrystals", *J. Rare Earth.*, **36** [10] (2018) 1060–1066.
47. S.H. Yoon, D. Liu, D. Shen, M. Park, D.J. Kim, "Effect of chelating agents on the preferred orientation of ZnO films by sol-gel process", *J. Mater. Sci.*, **43** [18] (2008) 6177–6181.
48. J. Miller, S. Veeramasuneni, J. Drelich, M. Yalamanchili, G. Yamauchi, "Effect of roughness as determined by atomic force microscopy on the wetting properties of PTFE thin films", *Polymer Eng. Sci.*, **36** [14] (1996) 1849–1855.
49. Z. Giedraityte, M. Tuomisto, M. Lastusaari, M. Karppinen, "Three-and two-photon NIR-to-Vis (Yb, Er) upconversion from ALD/MLD-fabricated molecular hybrid thin films", *ACS Appl. Mater. Interface*, **10** [10] (2018) 8845–8852.